



ELSEVIER



CrossMark

Procedia Manufacturing

Volume 5, 2016, Pages 734–746

44th Proceedings of the North American Manufacturing
Research Institution of SME <http://www.sme.org/namrc>



Enhancement in Photoconductivity of a-Si Thin Films by Annealing and Texturing Technique with the Third Harmonic Output from a Pulsed Nd³⁺:YAG Laser

Y. Esther Blesso Vidhya and Nilesh J. Vasa

Department of Engineering Design, Indian Institute of Technology, Chennai, 600036, India
estherblessoanand@gmail.com, njvasa@iitm.ac.in

Abstract

Influence of the third harmonic pulsed Nd³⁺:YAG laser on the formation of a polycrystalline-silicon (poly-Si) on a-Si thin film with thickness of 1000 nm and 400 nm in water and air ambience was investigated. In order to induce texturing of surface along with annealing, laser beam overlap technique with different percentages of spot overlap was used. Crystalline characteristics and electrical characteristics were studied to confirm the extent of crystallization. The crystalline characteristics of the film obtained with the Gaussian and the flat-top beam profiles were comparable for higher percentage of overlapping. Based on the theoretical modeling, the laser treatment without the ablation with the third output from the Nd³⁺:YAG laser was limited to the a-Si film thickness up to 800 nm. This was in qualitative agreement with the experimental observations.

Keywords: Laser annealing, amorphous silicon, Texturing, Thin films, Solar cells, Photoconductivity

1 Introduction

Solar photovoltaic technology is one of the most promising technologies to meet the increasing energy demand. Majority of solar cells use silicon as a material due to its efficiency, stability and availability (KL Chopra et al. 2004). However considering material benefit, heterostructure photovoltaic cell with amorphous silicon (a-Si) thin films is attractive as a-Si films possess a larger band gap (1.7 eV) than crystalline silicon (1.1 eV). Hence, cells can also absorb the visible part of the solar spectrum more effectively and offer material saving. However efficiency of a-Si films is limited due to the absence of crystal structure and the presence of dangling bonds which adversely affect the mobility resulting in low photovoltaic efficiency. This less efficient, but cost effective a-Si can be modified into polycrystalline silicon by inducing crystallization through laser annealing (Choi TY et al. 2003). Laser energy is used to heat the a-Si thin film, melting it and changing the microstructure to polycrystalline-Si as it cools. Compared to conventional furnace annealing, this localized laser annealing makes it possible to process thin films without affecting the substrate. Further, as reported

Enhancement in photoconductivity of a-Si thin films by annealing and texturing technique with the third harmonic output from a pulsed Nd³⁺:YAG Laser Esther Blesso Vidhya Y and Nilesh Vasa

by Palani IA et al.(2008), an increase in absorption of solar radiation on the surface of solar cell is useful in improving the efficiency of the solar cell. Simultaneously inducing texturing during laser annealing may assist in trapping and increase in absorption of solar light.

Laser annealing is a kinetic process where a short high intensity laser pulse is used to heat amorphous-silicon (a-Si) thin film in to a molten layer. The crystallized Si starts to grow as heated a-Si cools (Palani IA et al. 2008). Conventionally, excimer lasers, such as XeCl (308 nm), KrF (248 nm) lasers have been used for annealing of thin film solar cell (Azuma et al. 2002). The advantage of excimer lasers is the strong absorption of UV light in silicon and most of the laser energy is deposited close to the thin film surface (few tens of nm). So the thermal effect on the substrate is lower than that of lasers with longer wavelength. Recently, there has been a growing interest in using XeF (351 nm) for such applications as the photon energy of XeF laser (3.5 eV) is close to the binding energy of the Si-H bond (3.4 eV) as reported by Kuo C et al. (2006). In addition, excimer lasers have certain limitations, such as high operational cost and environmental problems due to its toxic nature. Alternatively, Nd³⁺:YAG laser with the third (355 nm) harmonics can be considered for the treatment of a-Si films.

Extensive work on laser surface texturing of crystalline silicon had been reported by different groups like Crouch CH et al.(2004), Iyengar VV et al. (2011) and Halbwx M et al.(2008). However, limited work is presented for the simultaneous annealing and texturing of a-Si thin films in different ambience like air and water (Wang H et al. 2012, Palani IA et al. 2008, Nayak BK et al. 2007). Most of the studies concerned utilize femtosecond lasers on silicon wafers or a-Si thin films, but they involve ablation induced surface structuring. There are no studies reported on simultaneous wide-area annealing and texturing of thick (> few hundred nm) a-Si films in water ambience using a Q-switched, nanosecond pulsed Nd³⁺:YAG laser with a wavelength of 355nm. This laser-assisted melting and re-solidification approach induces the texture formation via capillary action in molten silicon without ablating the material. The laser beam profile used for the laser treatment is also expected to influence the crystalline and electrical characteristics of poly-crystalline thin films. When a Gaussian beam is used, only a part of the energy will be effectively utilized and results in non-uniform annealing. Flat-top profile which has uniform intensity distribution can also be considered (Esther et al. (2015)).

In this paper, the influence of third harmonic (355 nm) of Nd³⁺:YAG laser on simultaneous annealing and texturing of a-Si thin films in different ambience and beam profiles is studied. Wide area annealing and texturing is achieved by scanning the surface with different percentages of spot overlapping. A two-dimensional thermal model has been used for estimating the rise in thin-film temperature for different fluence values to establish the operational range and the crystallization depth that can be achieved during the process for the wavelength of 355nm.

2 Experimental Details

Figure 1 shows the experimental setup. Simultaneous laser annealing and laser nano- texturing was performed using a solid-state pulsed Nd³⁺:YAG laser (Brilliant b, Quantel) at third harmonics (355 nm), with a frequency of 1 Hz and a pulse width of 5 ns (FWHM). Two different types of laser-beam profile, namely Gaussian, and flat-top intensity distribution were used. The laser beam was focused to form a spot size of 2 mm diameter on a-Si film by using a lens of focal length 200 mm. Experiments were performed in different ambient conditions, such as in air and under-water to determine appropriate conditions for annealing and texturing of a-Si films. For underwater treatment, the samples were kept under 3 mm depth of deionized water. Samples were scanned by moving the sample with a X-Y stage and the laser position was fixed. A beam shaper (Pi-Shaper 12_12_355_HP, AdlOptica) was used to change the Gaussian output from the laser into a flat-top beam profile. 10 mm × 10 mm samples were scanned using the laser with different percentage of spot overlapping. The speed of X-Y

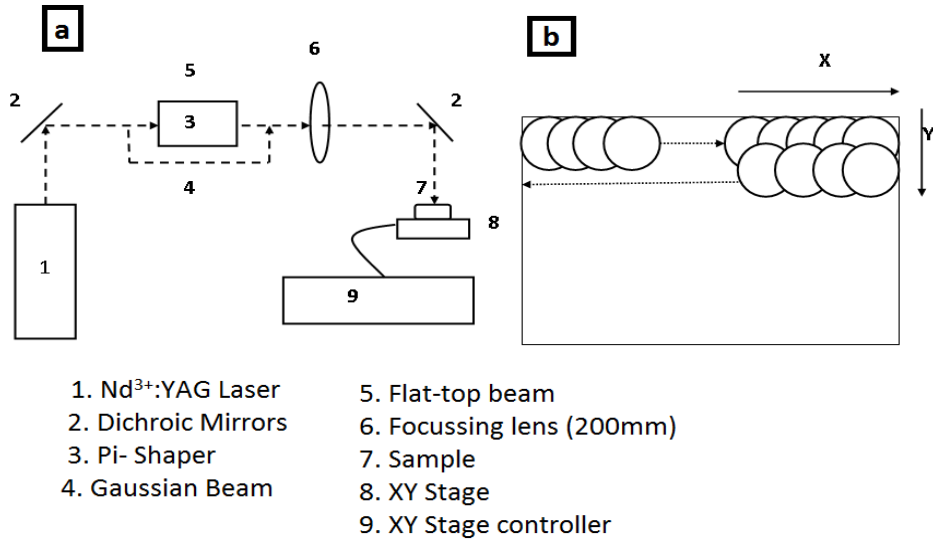


Figure 1. (a) Experimental setup for nanosecond Laser annealing with Flat-top and Gaussian beams (b) Laser annealing and texturing with spot overlap.

stage movement was controlled to get the desired spot overlapping. To maintain uniformity, the overlapping was done along the Y axis also after completing the processes along the X-axis.

Laser treated thin films were characterized by scanning electron microscope (SEM) (FEG, Quanta 400) to analyze the surface morphological changes. Raman spectroscopy (Jusco 5000 series) and the X-ray diffraction (XRD) (Discover D8, Bruker) techniques were used to investigate the crystallization characteristics and the extent of crystallization for different experimental conditions.

Raman spectroscopy is based on inelastic scattering of monochromatic light, usually from a laser source in which the frequency of photons in monochromatic light changes upon interaction with a sample. The frequency is shifted up or down in comparison with original monochromatic frequency, depending upon the vibrational state of the molecule in the sample under study. This shift provides chemical and structural information about a sample which include changes of crystallinity and phase across the sample. In the Raman spectra, highly crystalline regions show a distinct-peak with a narrow width (few cm⁻¹) whereas amorphous regions have a broader width (few tens of cm⁻¹). Crystallization of amorphous materials leads to the narrowing of amorphous band and corresponding Raman shift towards the frequency of crystalline peak. Narrowing of the spectra also confirms crystalline phase.

The atoms in a crystal are arranged in a periodic array and thus can diffract light. The scattering of

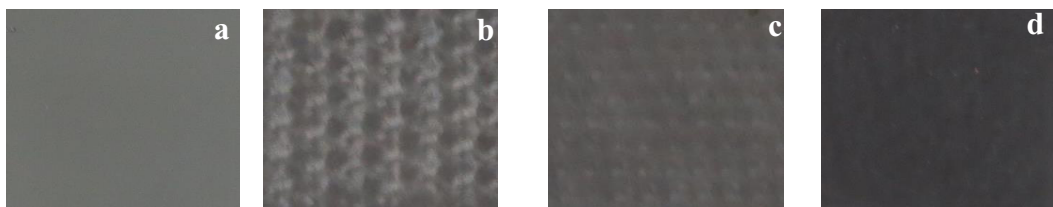


Figure 2. Photographic images of (a) untreated and treated a-Si / c-Si samples of size 10 mm × 10 mm with a spot overlap of (b) 30% (c) 50% (d) 90% in water with a fluence of 400 mJ/cm² showing darkening of the surface with the increase of overlapping.

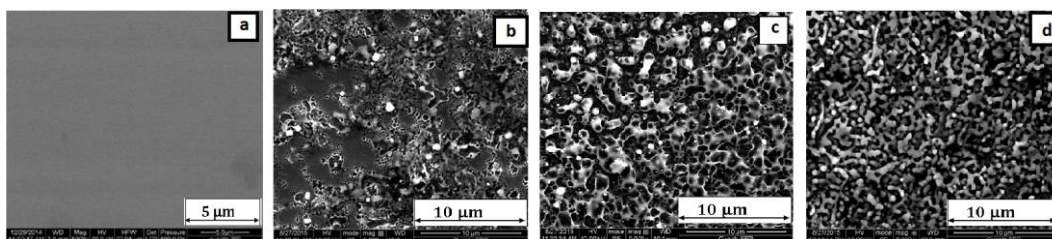


Figure 3. SEM images of (a) untreated and treated a-Si / c-Si samples with a spot overlap of (b) 30% in water (c) 30% in air (d) 90% in water with a fluence of 200 mJ / cm² and Gaussian beam profile (Images with 5000X magnification).

X-rays from atoms in X-ray diffraction (XRD) technique produces a diffraction pattern, which contains information about the atomic arrangement within the crystal. Amorphous materials do not have a periodic array with long-range order, so they do not produce a diffraction pattern and therefore produces only broad scattering peak. After annealing, crystallinity of the films is confirmed by the presence of crystalline peaks and the quenching of amorphous broad band.

The four-point Kelvin probe method is the most common way to measure a semiconductor material's electrical characteristics. Two of the probes are used to source current to the material and the other two probes are used to measure voltage. Using four probes instead of two probes eliminates measurement errors due to the probe resistance, the spreading resistance under each probe, and the contact resistance between each metal probe and the specimen material. This technique involves bringing four probes at known distance and geometry into contact with the material. Electrical characteristics were analyzed by using the four-probe technique and current-voltage (I-V) measurements of treated and untreated samples were performed using an appropriate light source with an electrical source/ measurement unit (B2901A, Keysight).

3 Results and Discussions

Figure 2 shows the photographic images of untreated and laser treated a-Si / c-Si samples in water environment. When observed after laser treatment, the surface of the treated sample is much darker similar to black silicon (Sarnet T et al. 2015) compared to the shiny surface of the untreated film, which indicates that the treated surface has the capability to reduce reflection.

Scanning electron microscope (SEM) of the untreated and laser treated samples in water with different percentage of spot overlapping is shown in Figure 3. For untreated sample, no traces of surface patterns were observed. Laser annealing produced silicon with a rough surface morphology consisting of *sub-micrometer* size granular structures. The surface morphology after laser treatment

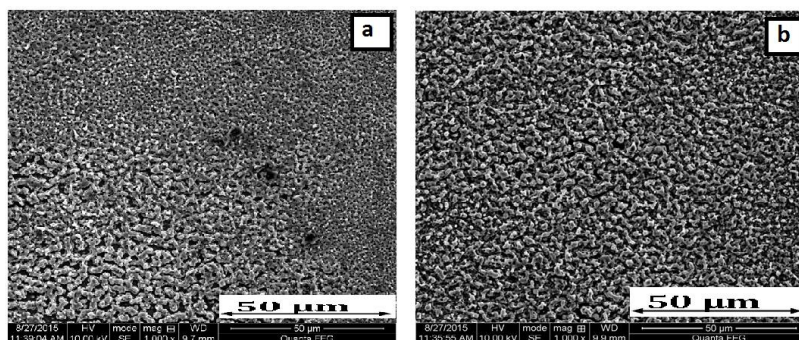


Figure 4. SEM images of a-Si / c-Si samples irradiated with 20 pulses of fluence 200mJ/cm² in air with (a) Gaussian and (b) flat-top beam profiles (Images with 1000X magnification).

depends on different parameters such as number of incident pulses (or percentage of overlapping), fluence values, laser beam profile and ambient conditions. Due to the absorption by water, the laser fluence available during underwater annealing was less than that of in air. Hence, for a 30% overlapping of the laser spot, randomly distributed smaller structures were produced as compared to that of air as shown in Figures 3(b) and (c). On the other hand, laser annealing with a larger percentage of overlap (90%) in water produced high density smaller textures compared to air (Figure 3(d)). To understand the effect of laser beam profile on surface morphology, samples irradiated with multiple pulses on the same spot with Gaussian and flat-top beams were analyzed with scanning electron microscope and the results are shown in Figure 4. In the case of the laser treatment with the Gaussian beam profile, regions with different sizes of bead like structures were produced as shown in Figure 4(a). On the other hand, laser treatment with the flat-top beam profile produced uniform change in surface morphology as shown in Figure 4(b).

After laser treatment, Raman spectroscopic studies were performed to analyze the crystallinity of the thin film. Figure 5 shows the Raman spectra of the samples before and after laser processing with different laser-fluence values for 1 μm thick a-Si coated on c-Si samples. Figure 5(a) shows the Raman spectra corresponding to the amorphous Si film and c-Si sample. In the case of untreated a-Si on crystalline silicon (a-Si/c-Si) sample, a peak around 501 cm⁻¹ and a broad peak of the amorphous phase around 480 cm⁻¹ was observed. In the case of c-Si sample, Raman spectral peak around 520 cm⁻¹ was observed. The peak is shifted from a typical value of around 470 cm⁻¹ corresponding to a-Si, which might be due to the effect of c-Si substrate. Nanosecond laser annealing reduced the amorphous

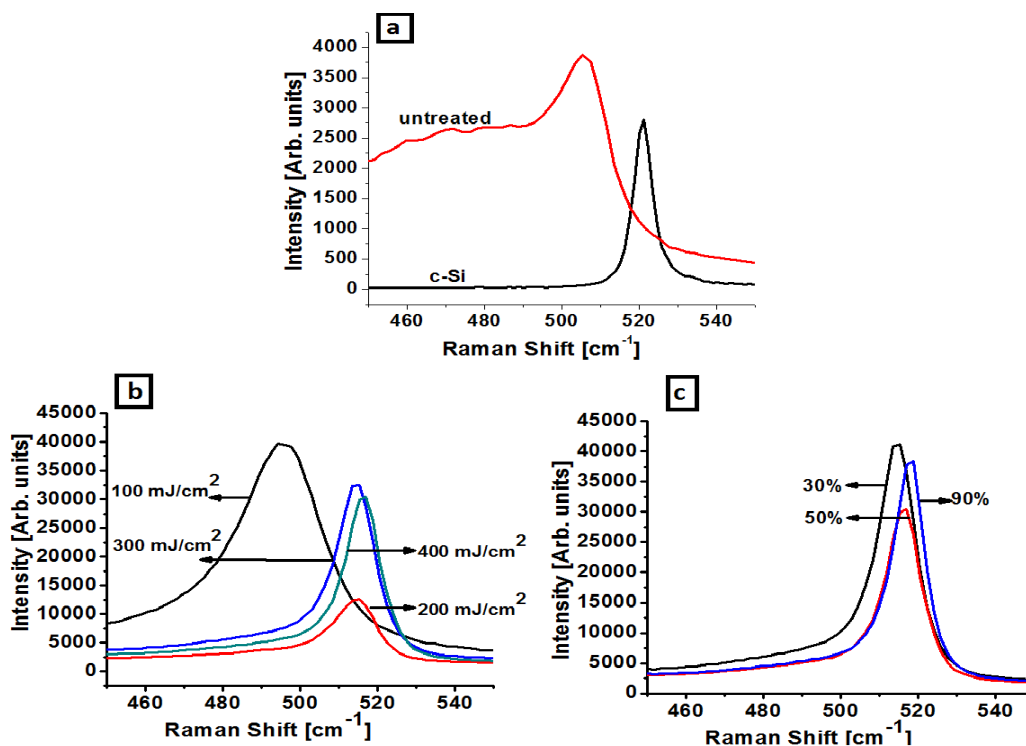


Figure 5. Raman spectroscopy of the (a) untreated and laser treated a-Si/c-Si samples in air at 355 nm with (b) with different fluence values for 50% spot overlap with Gaussian beam (c) different percentage of spot overlap with 400mJ/cm².

phases shown in Raman spectra. Figures 5(b) and (c) show the Raman spectra of the laser treated samples with the Gaussian beam profile in air. Based on Figure 5(b), corresponding to the laser fluence of 100, 200, 300 and 400 mJ/cm², shift in Raman peak values to 495, 515, 515 and 517 cm⁻¹, respectively, were observed around the crystalline peak value of 520 cm⁻¹ confirming the poly-crystalline nature of the film. As shown in Figures 5 (b) and (c), the spectral width was reduced, and the peak was shifted towards the c-Si peak with the increase in the laser fluence values. For different percentage of spot overlap, shift in Raman peak values to 515, 517 and 519 cm⁻¹ were observed for 30%, 50% and 90%, respectively. Further, reduction in the peak width was observed as the overlap percentage increased, which indicated the increase in the crystallinity.

In addition to Raman spectroscopic analysis, X-ray Diffraction (XRD) analysis was also performed so as to confirm the nature of crystallization and to determine the orientation of the grains. XRD measurements were performed in a symmetric θ -2 θ geometry with a Bruker D8 advance diffractometer operating with CuK α radiation ($\lambda=1.5418 \text{ \AA}$).

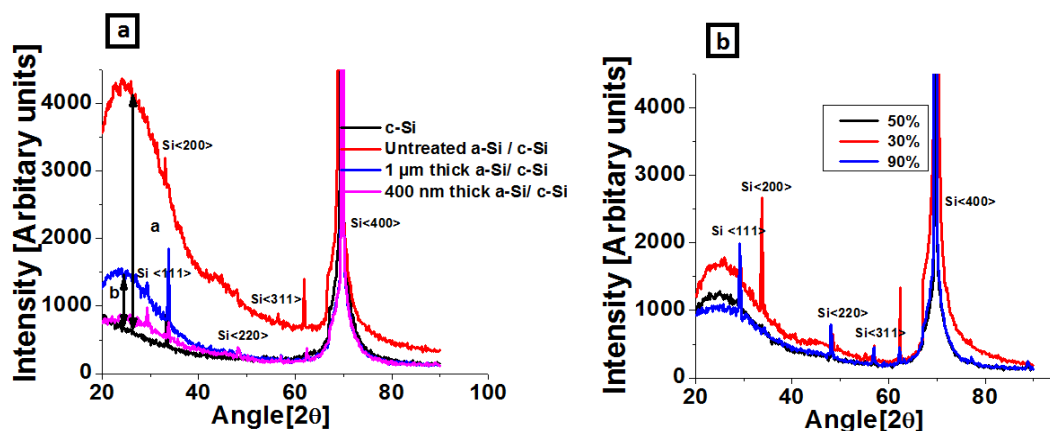


Figure 6. (a) XRD data of the untreated and laser treated a-Si/c-Si sample for the laser fluence of 200 mJ/cm² and Gaussian beam profile with 50% spot overlap (b) different percentages of spot overlap with 400 mJ/cm².

The X-ray diffraction patterns of untreated and laser treated a-Si/c-Si samples treated under different conditions are presented in Figure 6. All the spectra show an amorphous broad peak around 25°, which is caused by the internal constructive interference of the a-Si. The broad-band XRD patterns in Figure 6 show that the untreated sample was amorphous. The crystalline substrate peak is observed at 69.15°, which corresponds to (400) peak for Si. An additional peak at ~ 33° has been observed on all the Si (100) substrates, which corresponds to Si (200) planes. (Gupta A et al.2004). After laser annealing, as shown in Figure 6 (a) and (b), diffraction peaks were observed at 28.4°, 47.3° and 56.1° and identified as (111), (220), and (311) peaks of Si. When the laser fluence value was increased to 450 mJ/cm², the broad spectrum of amorphous silicon was quenched. The presence of Si peaks (111), (220), and (311) confirmed the poly-crystalline nature of the film. The improved crystallinity in the treated samples was calculated based on the quenching of the amorphous band around 25° after laser treatment by taking XRD pattern of c-Si as reference. The percentage of improvement from

Sample	Fluence	% of improvement
30%, 1 μ m	400mJ/cm ²	~ 72%
50%, 1 μ m	400mJ/cm ²	~ 82%
90%, 1 μ m	400mJ/cm ²	~ 88%
50%, 1 μ m	200mJ/cm ²	~ 77%
50%, 400nm	200mJ/cm ²	~ 95%

Table 1: Percentage improvement in crystallinity based on XRD measurements

Enhancement in photoconductivity of a-Si thin films by annealing and texturing technique with the third harmonic output from a pulsed Nd³⁺:YAG Laser Esther Blesso Vidhya Y and Nilesh Vasa

amorphous towards crystalline for the samples treated under different conditions is listed in Table 1. It was calculated by using a formula $\frac{a-b}{a} \times 100\%$, where a and b are intensity of untreated a-Si and laser treated samples, respectively, corresponding to the XRD pattern of c-Si at the angle of 25°. Almost 95% quenching of amorphous band was observed for a-Si thin film with a thickness of 400 nm when compared to 1 µm. Thus third harmonics is suitable for the crystallization of up to few hundreds of nm thin film.

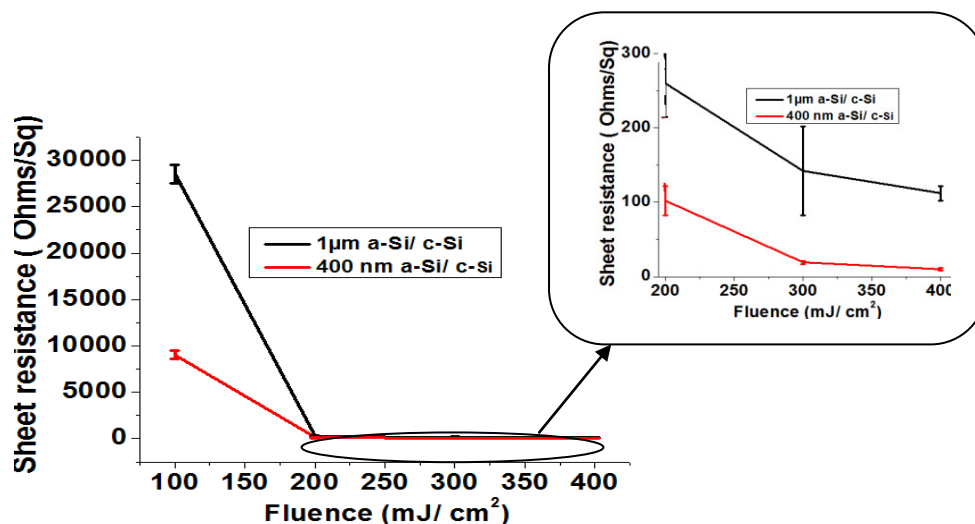


Figure 7. Resistance of ns- laser treated samples at the wavelength of 355 nm treated with different fluences with 30 % of spot overlap in air.

3.1 Electrical Characterization

Four probe resistance measurement of treated and untreated samples were performed using a source /measurement unit (B 2901A, Keysight). The sheet resistance of a-Si/c-Si samples without laser annealing is found to be around 900 MΩ/Sq. The Nd³⁺:YAG laser annealing improved the crystalline characteristics of a-Si films and the overall sheet resistance of the film was decreased. When the samples were treated at the wavelength of 355 nm with 30% spot overlap, the sheet resistance was found to be below 500 Ω/ Sq, for the laser fluence ranging from 200 to 400 mJ/cm² and 400 nm thick a-Si films showed less sheet resistance compared to 1µm a-Si film as shown in Figure 7.

Photovoltaic properties, such as photoconductivity of the laser treated and nano-textured samples were investigated. I-V characterization was performed by illuminating the laser treated sample with a Xe light source with the power of 250 Watts. Current and voltage measurements were performed with the precision source /Measurement unit (B2901A ,Keysight). Figure 8 (a) and (b) shows current-voltage measurements of laser treated samples. The input intensity of the light illuminating the sample surface is 1426 W/ m². The value of the open circuit voltage V_{oc} (voltage when current is zero) and the short circuit current I_{sc} (current when voltage is zero) were higher with the 30% overlapping as compared to that of 50% overlapping. This might be due to the change in the film characteristics. The ablation threshold might have decreased with increasing number of pulses due to change of the absorption behavior of the film. Overall, the textured surface significantly improved the amount of incident light absorption through multiple-reflections. The maximum power delivered by the untreated sample was ~ 8.88 × 10⁻⁶ W. After laser treatment, maximum power in the order of milliwatts was

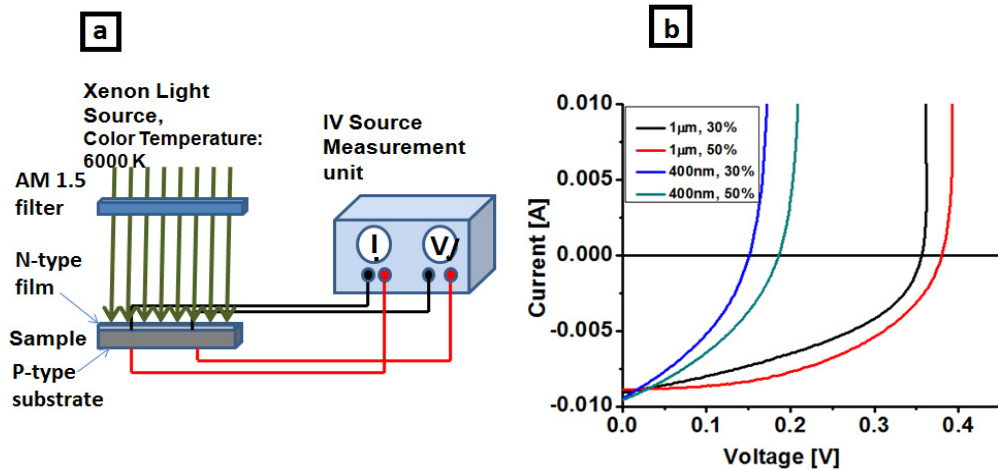


Figure 8. (a) IV measurement setup and (b) IV characteristics of laser treated PN photovoltaic cell under illumination with Gaussian beam profile in air with 200mJ/cm².

observed. Different parameters observed from I-V characterization and efficiency by the laser treated PN photo voltaic cell with fluence value of 200 mJ/ cm² are listed in Table 2. Higher output efficiency was observed with 1µm thick samples when compared to the 400 nm thick samples. Improvement in Voltage and Current values were observed after annealing and the value of the maximum power from air treated samples produced better or comparable results with underwater treated samples in low fluence window whereas samples treated with high fluence in water delivered more power compared to that of air treatment. Slight Improvement in the efficiency was derived from flat-top beam annealed samples than Gaussian treated samples.

Sample	Ambience	J _{sc} (mA/ cm ²)	V _{oc} (V)	Fill factor	Efficiency (%)
1 µm, 30%, Gaussian	air	9.1	0.36	0.4	0.98
400 nm, 30%, Gaussiar	"	9.5	0.15	0.35	0.35
1 µm, 50%, Gaussian	"	8.9	0.38	0.5	1.2
1 µm, 50%, flat-top	"	13.4	0.3	0.5	1.3
1 µm, 30%, Gaussian	water	8.5	0.25	0.56	0.8
1 µm, 50%, Gaussian	"	10.5	0.31	0.6	1.5
1 µm, 50%, flat-top	"	9.6	0.41	0.61	1.7

Table 2: Current (I) - Voltage (V) characterization data and efficiency by the laser treated PN photo voltaic cell with fluence 200 mJ/ cm².

4 Theoretical Analysis

When the high intense laser pulse of nano-second order interacts with the material, high energy photons get absorbed by the material, which excites the carriers to a higher level. After a certain life time, carriers transfer its energy to the lattice through a relaxation process and hence lattice is getting heated through the phononic vibration. In other words, the absorbed laser energy is instantaneously converted to local heat, which can diffuse by thermal conduction. So the heat distribution varies with depth and time. When the laser fluence crosses the threshold, layers that lies in the crystallization temperature region melt and get crystallized. Depending on the laser fluence, the vaporization temperature can be reached at the irradiated region, and the ablation effects are expected. The numerical model helps to establish the fluence range needed for melting and crystallization without any damage or ablation of the thin film.

The heating process in the a-Si thin film is governed by the thermal model with heat conduction equation (Garcia O et al. 2013). In this model, thermal state of the material is determined by the properties such as material density, thermal conductivity, specific heat capacity and absorption coefficient. As a circular beam profile was considered, the heat distribution was expected to be symmetric about the vertical axis, and the simulation studies were performed with a two-dimensional model. The influence of the laser pulse along with the reflectivity parameter was incorporated in the model through a heat source term. The absorbed light energy in a-Si thin film is converted into accumulated heat energy in each layer and conducted thermal energy to the next layer with respect to time, and this process can be simulated by the heat transfer equation. Figure 9 shows the flowchart for the theoretical modelling. In the flowchart, T is the temporal and spatial temperature distribution, $c(T)$

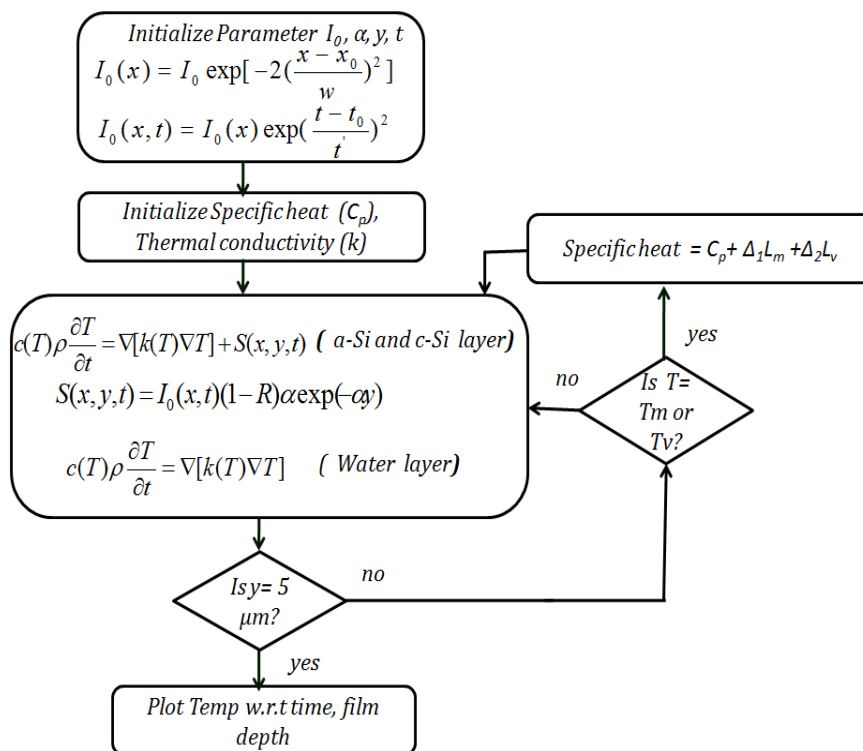


Figure 9. Flow chart for the numerical analysis with heat transfer equation.

Physical properties	a-Si	c-Si
Density(kg/m ³)	2330	2380
Thermal Conductivity (W/mK)	$1.3 \times 10^{-9}(T-900)^3 + 1.3 \times 10^{-7}(T-900)^2 + 1 \times 10^{-4}(T-900) + 1$	$29900/(T-99)$
Specific heat (J/kg.K)	$952 + 171T/685$	880
Reflectivity	0.54 @ 355nm 0.4 @ 532nm	0.6 @ 355 nm 0.36 @ 532 nm
Melting point (K)	1420	1685
Boiling point (K)	2628	
Latent Heat (melting) (J/g)	1320	
Latent Heat (vaporization)(J/g)	13.6×10^3	

Table 3: Physical properties considered for this modelling

is the specific heat, ρ is the material density, k is the thermal conductivity and $S(x,y,t)$ is the source term that determines the way the laser radiation is absorbed by the material. The specific heat ($c(T)$) of a-Si is replaced by $C_p + \Delta L_m + \Delta L_v$ in the heat-transfer equation where C_p is the specific heat of a-Si, L_m and L_v are latent heat of melting and vaporization respectively. A Gaussian function $\frac{1}{\sqrt{\pi}dT} \exp\left(-\frac{(T-T_x)^2}{dT^2}\right)$ was considered as phase change function Δ where T_x is T_m (Melting Temperature) or T_v (Vaporization Temperature) of a-Si. The source term refers to the incident laser pulse which was assumed to be Gaussian both in temporal and spatial beam profile for the Gaussian intensity distribution and for the flat-top distribution, spatial profile was assumed to be uniform. The absorbed energy along the depth depends on the exponential decrease in the intensity as per the Beer-Lambert's law. α and R are the wavelength dependant absorption coefficient and the reflectivity of the material, respectively and t_{pulse} represents half the pulse width, which corresponds to full width at half maximum (FWHM). The energy loss due to the Planck radiation, surface evaporation at the melting point and heat convection to the surroundings is very small in comparison with the laser beam intensity and therefore, is not included in the source term ($I_{loss} < 10^{-3} I_0$).

4.1 Simulations & Results

In the simulation, a-Si film thickness of 1 μm on the c-Si substrate was considered. The laser beam diameter is considered to be 2 mm and the FWHM pulse duration is 6 ns. Initially the temperature of the sample is equal to the ambient temperature (300 K). So the initial and boundary conditions are $T(y,t)|_{t=0} = 300\text{K}$, $T(y,t)|_{y=\alpha} = 300\text{K}$ and $\frac{\partial T}{\partial t}|_{y=0} = 0$ where $T(y,t)$ is the temperature distribution, y is the depth direction from the surface. The expressions and parameters considered for this modelling are shown in Table 3. Experimentally measured absorption coefficient was used. For underwater modelling, Convective heat flux to water was considered at the side boundaries, and a water layer of 5 μm thick was considered above the thin film. Single pulse laser annealing was considered, and the temperature distribution was estimated at the wavelengths of 532

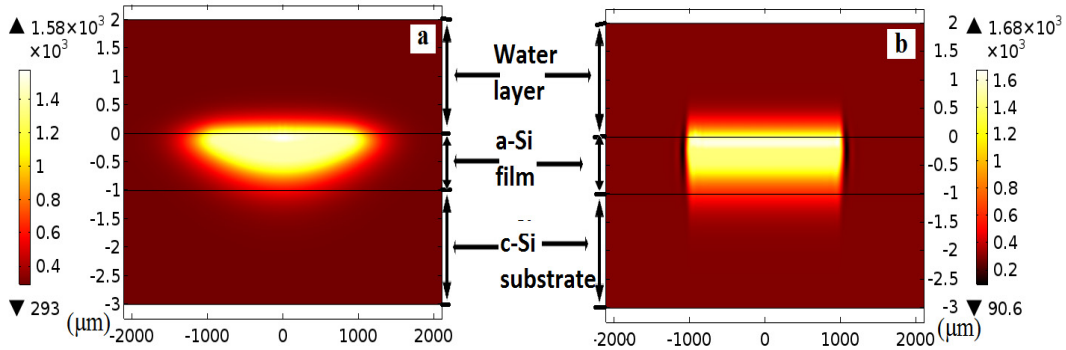


Figure.10 Temperature distribution profile in two dimensional for (a) Gaussian beam and (b) flat-top beam for 400 mJ/cm².

nm and 355 nm for varying laser fluence values to understand the effect of wavelength. The effect of water cooling, the temperature rise at the irradiated surface and the crystallization depth were studied. The expressions and parameters considered for the modelling are described in Table 3.

Theoretical simulation was performed using the COMSOL Multiphysics (version 4.4). The fluence range and depth of crystallization were calculated by considering the crystallization temperature range of a-Si from 1073 K to the boiling point (2628 K) (Kawazu Y et al. 1990).

Figures 10 (a) and (b) show the cross section of water-film-substrate layer and the two dimensional temperature distributions along depth across the cross section from the centre of the laser beam at 10 ns after laser irradiation for the Gaussian beam profile and the flat-top beam profile, respectively, corresponding to a typical laser fluence of 400 mJ/cm². The heat generated by the absorption of laser energy is redistributed by heat conduction inside the thin film and towards the water. The maximum temperature is reached at a depth nm instead of thin film surface because of the water cooling at the film-water layer interface whereas maximum temperature was calculated at the surface of the thin

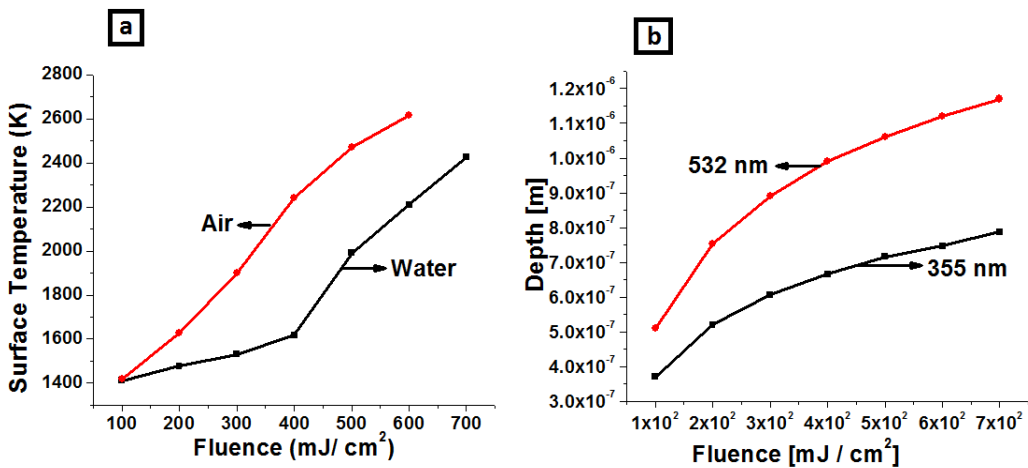


Figure 11. (a) Temperature rise during laser irradiance at the surface for different laser fluence in air and water (b) Depth of crystallization with different fluence values with 532 nm and 355nm.

Enhancement in photoconductivity of a-Si thin films by annealing and texturing technique with the third harmonic output from a pulsed Nd³⁺:YAG Laser Esther Blesso Vidhya Y and Nilesh Vasa

film in the case of laser annealing in air. The rise in temperature was uniform across the irradiated spot with the flat-top profile, therefore uniform annealing is expected.

Figure 11 (a) shows rise in surface temperature when a ns laser pulse of 355 nm irradiates on the sample with different laser fluences. From the fluence values of 100 mJ / cm² to 400 mJ / cm², the maximum surface temperature remains around 1400 K due to latent heat process and the phase change duration increases with increase in fluence. Complete melting occurs around 400 mJ / cm². From 400 mJ/cm² to 600 mJ/cm² surface temperature increases linearly with fluence till it reaches boiling point. The crystallization fluence range was estimated to be in between 100 mJ / cm² to 600 mJ/cm².

Figure 11 (b) shows the depth of crystallization that can be achieved with single pulse annealing. Based on the theoretical modeling, with the laser wavelengths of 532 nm and 355 nm, the maximum crystallization depth was calculated to be ≈1000 nm and ≈800 nm, respectively.

5 Conclusion

The influence of all solid-state, pulsed Nd³⁺:YAG laser with the wavelength of 355 nm in the annealing and texturing of a-Si films on crystalline silicon substrates has been investigated with different laser fluence values experimentally and theoretically. The laser fluence for efficient conversion from a-Si to polycrystalline silicon films was estimated to be between 100 and 600 mJ/cm² which is in good agreement with the experimental observations and the laser fluence for ablation threshold was estimated to be above 600 mJ/cm². The amount of heat incident on the surface was analyzed by solving two-dimensional heat equation, and the crystallization depth attained at different fluences was estimated. The percentage improvement in crystallinity with the suppression of the amorphous band was estimated to be ≈88% and ≈97% for the film thickness of 1000 nm and 400 nm, respectively. The crystalline characteristics of the film after laser annealing with higher percentage of overlapping using the Gaussian, and the flat-top beam profiles were comparable. The 1μm thick samples showed higher value of maximum power when compared to the 400nm thick samples in photoconductivity measurements. Improvement in V and I values were observed and the value of the maximum power increased for underwater treated samples when compared to that of air treated samples for higher laser fluence. Based on the theoretical modeling, the laser treatment without the ablation with the third harmonic (355 nm) output from the Nd³⁺:YAG laser is limited to the a-Si film thickness up to 800 nm.

References

- Azuma H, Takeuchia A, Ito T, Fukushima H, Motohiroa T and Yamaguchi M. Pulsed KrF excimer laser annealing of silicon solar cell. *Solar Energy Materials and Solar Cells* 2002; 74: 289-294.
- Chopra KL and Das SR. Thin-film solar cells: an overview. *Progress in Photovoltaics: Research and Application* 2004; 12: 69-92.
- Crouch CH, Carey JE, Warrender JM, Aziz MJ, Mazur E and Genin FY. Comparison of structure and properties of femtosecond and nanosecond laser-structured silicon. *Applied Physics Letters* 2004; 84: 1850-1852.
- Choi TY, Hwang DJ and Grigoropoulos CP. Ultrafast laser-induced crystallization of amorphous silicon films. *Optical Engineering* 2003; 42 (11): 3383-3388.
- Esther Y, Sriram R and Vasa NJ. Influence of Laser Beam Profile on Nd³⁺:YAG Laser Assisted Formation of Polycrystalline-Si Films in Underwater Conditions. *Journal of Laser Micro/Nanoengineering* 2015; 10 (3): 334-339.
- Gupta A, Paramanik D, Varma and Jacob C. CVD growth and characterization of 3C-SiC thin films. *Bulletin of Material Sciences* 2004; 27 (5): 445-451.

- Enhancement in photoconductivity of a-Si thin films by annealing and texturing technique with the third harmonic output from a pulsed Nd³⁺:YAG Laser Esther Blesso Vidhya Y and Nilesh Vasa
- García O, García-Ballesteros JJ, Muñoz-Martin D, Núñez-Sánchez S, Morales M, Carabe J, Torres I, Gandía JJ and Molpeceres C. Analysis of wavelength influence on a-Si crystallization processes with nanosecond laser sources. *Applied Surface Science* 2013; 278: 214–218.
- Halbwax M, Sarnet T, Delaporte P, Sentis M, Etienne H, Torregrosa F, Vervisch F, Perichaud I and Martinuzzi S. Micro and nano-structuration of silicon by femtosecond laser: Application to silicon photovoltaic cells fabrication. *Thin Solid Films* 2008; 516 (20): 6791-6795.
- Iyengar VV, Nayak BK, More KL, Meyer HM, Biegalski MD, Li JV and Gupta MC. Properties of ultrafast laser textured silicon for photovoltaics. *Solar Energy Materials and solar cells* 2011; 95 (10): 2745-2751.
- Kawak Y, Kudo H, Onari S, Arai T. Low-Temperature Crystallization of Hydrogenated Amorphous Silicon Induced by Nickel Silicide Formation. *Japan Journal of Applied Physics* 1990; 29:2698-2700.
- Kuo C, Yeh W, Chen J and Jeng J. Monitoring explosive crystallization phenomenon of amorphous silicon thin films during short pulse duration XeF excimer laser annealing using real-time optical diagnostic measurements. *Thin Solid Films* 2006; 515 (4): 1651-1657.
- Nayak BK and Gupta MC. Femtosecond-laser-induced-crystallization and simultaneous formation of light trapping microstructures in thin a-Si: H films. *Applied Physics A* 2007; 89:663-666.
- Palani IA, Vasa NJ and Singaperumal M. Crystallization and ablation in annealing of amorphous-Si thin film on glass and crystalline-Si substrates by third harmonics of Nd³⁺: YAG laser. *Material Science in Semiconductor Processing* 2008; 11: 107-116.
- Sarnet T, Carey J and Mazur E. From black silicon to photovoltaic cells, using short pulse lasers. *AIP Conference Proceeding*, 2012, 1464: 219-228.
- Tsunoda I, Matsuura R, Tanaka M, Watakabe H, Sameshima T and Miyao M. Direct formation of strained Si on insulator by laser annealing. *Thin Solid Films* 2006; 508: 96-98.
- Wang H, Lusquiños F and Yao YL. Effect of hydrogen on surface texturing and crystallization of a-Si:H thin film irradiated by excimer laser. *Applied Physics A* 2012; 107 (2): 307-320.
- Wang XC, Zheng HY, Tan CW, Wang F, Yu HY and Pey KL. Femtosecond laser induced surface nanostructuring and simultaneous crystallization of amorphous thin silicon film. *Optics Express* 2010; 18 (18): 19379-85.